bioRxiv preprint doi: https://doi.org/10.1101/2022.11.28.518189; this version posted December 2, 2022. The copyright holder for this preprint (which was not certified by peer review) is the author/funder. All rights reserved. No reuse allowed without permission.

A versatile method to archive and delipidate brain tissues for ensuing multiplexed immunolabeling and organ-level imaging

Ya-Hui Lin[1,2], Li-Wen Wang[1,2], Yen-Hui Chen[3], Yi-Chieh Chan[1], Shang-Hsiu Hu[1], Sheng-Yan Wu[1], Chi-Shiun Chiang[1], Guan-Jie Huang[2,4], Shang-Da Yang[2,5], Shi-Wei Chu[2,4] , Kuo-Chuan Wang[6], Chin-Hsien Lin[7], Pei-Hsin Huang[8], Hwai-Jong Cheng[9], Bi-Chang Chen[10,*] & Li-An Chu[1,2,*]

1. Department of Biomedical Engineering and Environmental Sciences, National Tsing Hua University, Hsinchu, Taiwan
2. Brain Research Center, National Tsing Hua University, Hsinchu, Taiwan
3. Institute of Biomedical Sciences, Academia Sinica, Taipei, Taiwan
4. Department of Physics, National Taiwan University, Taipei, Taiwan
5. Institute of Photonics Technologies, National Tsing Hua University
6. Department of Neurosurgery, National Taiwan University Hospital, College of Medicine, National Taiwan University, Taipei, Taiwan
7. Department of Neurology, National Taiwan University Hospital, College of Medicine, National Taiwan University, Taipei, Taiwan
8. Department of Pathology, National Taiwan University Hospital, Taipei, Taiwan
9. Institute of Molecular Biology, Academia Sinica, Taipei, Taiwan
10. Research Center for Applied Sciences, Academia Sinica, Taipei, Taiwan

bioRxiv preprint doi: https://doi.org/10.1101/2022.11.28.518189; this version posted December 2, 2022. The copyright holder for this preprint (which was not certified by peer review) is the author/funder. All rights reserved. No reuse allowed without permission.

Abstract

Current tissue clearing and labeling approaches require freshly prepared samples to avoid problems related to over-fixation, such as loss of antigenicity or difficulty of tissue clearing. Thus, the predicament of specimens with long-term preservation limits the application of state-of-art technology to archived human brain tissues. Here, we present the development and validation of multiplex labeling of centimeter-sized archived tissue (MOCAT)—a formalin-fixed paraffin-embedding (FFPE)–based sample preservation and delipidation technique for centimeter-level tissue clearing and immunolabeling. We demonstrate that MOCAT sufficiently delipidates whole mouse brain and human brain blocks and is superior to 10% formalin for long-term antigenicity preservation; moreover, the spatial information of biomarkers offered by MOCAT-processed intact mouse brains is identical to that offered by freshly prepared SDS-delipidated intact mouse brains. MOCAT not only satisfies the need for long-term tissue storage before performing volumetric multiplex imaging for research purposes but also has the potential to be used in human clinical examination.

bioRxiv preprint doi: https://doi.org/10.1101/2022.11.28.518189; this version posted December 2, 2022. The copyright holder for this preprint (which was not certified by peer review) is the author/funder. All rights reserved. No reuse allowed without permission.

Introduction

The fact that the brain functions as an organic entirety necessitates whole-brain imaging in neuroscientific or clinical brain research. This requirement may be fulfilled by the recent advancements in tissue clearing techniques[1–8]. Large tissue clearing techniques combined with immunolabeling[9–12] and genetic tools[13] capable of labeling specific proteins, cells, or neurons, enable volumetric imaging of an intact mouse brain and provide brain-wide information that cannot be obtained from conventional histological approaches[14–17]. However, current large tissue clearing approaches did not suggest an appropriate way to preserve samples that need to be archived for future three-dimensional (3D) imaging. Human brain banks usually archive precious human tissues in formalin or ultra-low temperature freezers. However, both ways are unsuitable for large tissue clearing and immunolabeling because stable crosslinks caused by long-term formalin preservation hinder immunolabeling[18], and frozen tissues suffer from damage caused by thawing. This limitation makes researchers opt for tissue sections and contradicts research using archived human brains. Therefore, a new method is required to bridge the gap between the need for long-term tissue preservation and further organ-level multiplex imaging in cellular resolution.

Paraffin embedding is a standard technique commonly used in clinical and research laboratories for tissue archiving. After adequate fixation, biological samples can be dehydrated and preserved in formalin-fixed paraffin-embedded (FFPE) blocks for years at room temperature. Besides, the widespread use of FFPE tissue sections for immunohistochemistry suggests that proteomic information can be preserved in pristine condition[19]. Furthermore, a substantial amount of lipids would be removed by xylene during the paraffin embedding process. These advantages led us to investigate its potential for long-term preservation and delipidation of the brain tissue before whole-mount immunolabeling. Here, we developed multiplex labeling of centimeter-sized archived tissue (MOCAT), a paraffin-processing-based versatile technique for preservation and delipidation.

Results

Heat-induced antigen retrieval removed lipids remained after dewaxing

Although xylene removed a significant amount of lipids, studies have indicated that phospholipids and myelinated lipids are retained after FFPE processing and dewaxing possibly due to crosslinking with surrounding proteins[20]. To unmask crosslinked antigens, pathological laboratories usually use proteolytic or heat-induced methods termed

bioRxiv preprint doi: https://doi.org/10.1101/2022.11.28.518189; this version posted December 2, 2022. The copyright holder for this preprint (which was not certified by peer review) is the author/funder. All rights reserved. No reuse allowed without permission.

antigen retrieval[21]. Because increasing temperature reinforce detergent diffusion into tissues[6], we hypothesized that heat-induced antigen retrieval with additional detergent can remove remaining lipids from dewaxed FFPE tissues by releasing protein-linked lipids and membrane phospholipids. To verify the hypothesis, we adopted a modified heat-induced antigen retrieval method (see Methods) and used coherent anti-Stokes Raman scattering (CARS), a spectroscopic technique used to detect vibrational responses of specific molecular structures, to assess the remained lipid amount of mouse brain samples (Fig. 1a). We found that axon bundles in striatum was bright in a dewaxed FFPE mouse brain (Fig. 1a, left), indicating myelinated lipids existence; however, antigen retrieval removed most remained lipids successfully (Fig. 1a, middle). The results also showed that the steps of paraffin embedding, dewaxing and antigen retrieval has similar delipidation ability to SDS-based electrophoresis (Fig. 1a, middle and right), indicating that the conventional SDS-based delipidation step in aqueous tissue clearing could be replaced by paraffin embedding, dewaxing, and antigen retrieval. To speed up immunolabeling and protect samples from the harsh conditions of multiplexed staining, we combined the stabilization to harsh conditions via intramolecular epoxide linkages to prevent degradation (SHIELD) procedure[22] and electrophoretic immunolabeling[11] into MOCAT pipeline (Fig. 1b).

MOCAT reveal proteomic spatial information for 3D visualization as well as conventional SDS-delipidation

To demonstrate that paraffin blocks preserve spatial information, we performed immunolabeling on one MOCAT-processed mouse brain, and one 24-hour 4% paraformaldehyde (PFA) fixed and SDS-delipidated (hereinafter referred to as SDS-delipidated) mouse brain. Immunolabeling with tyrosine hydroxylase (TH, a dopaminergic neuronal marker) antibodies revealed dopaminergic neuronal distribution in the striatum, nigrostriatal fiber tracts, substantia nigra, ventral tegmental area, pontine reticular nucleus, and lateral reticular nucleus (Fig. 1c). MOCAT- and SDS-delipidated mouse brains showed identically labeled structures, demonstrating that FFPE blocks preserve spatial information comparable to 24-hour PFA-fixed brains. To prove that MOCAT could be applied on already archived samples, we applied this method to a 15-year-old, 2-mm-thick FFPE block (Fig. 1d). The brain regions containing dopaminergic neurons were identified (Fig. 1e), and the morph of individual dopaminergic neurons was observed (Figs. 1f). The results indicated that three-dimensional (3D) expression patterns of biological markers could be preserved for decades and revealed later by performing MOCAT. Notably, the dewaxing time should be increased when working with a large sample; otherwise, the residual wax from insufficient dewaxing would cause opacity. The opacity could be restored through

bioRxiv preprint doi: https://doi.org/10.1101/2022.11.28.518189; this version posted December 2, 2022. The copyright holder for this preprint (which was not certified by peer review) is the author/funder. All rights reserved. No reuse allowed without permission.

repeated dehydration and dewaxing (Supplementary Fig. 1b), and repeated dewaxing and prolonged dewaxing time did not affect tissue structure or antigenicity (Supplementary Figs. 1 and 2).

MOCAT enables multiplexed immunolabeling

Multiplex immunostaining is essential to further investigating molecule interactions and the microenvironment. However, the number of biological markers labeled in a single round is typically limited by antibody host species and the fluorescent spectrums of excitation/emission wavelength. To overcome this limitation, MOCAT includes a step for multiple rounds of immunostaining on a single whole mouse brain (Fig. 1b). To maintain the fluorescent signals, we postfixed the labeled sample with 4% PFA after each round of immunolabeling (Supplementary Fig. 3). After imaging completed, the RI-matched transparent sample were photo-bleached by LED white light. To release the re-masked epitopes by the postimmunolabeling fixation, we than performed another round of antigen retrieval (Fig. 2a and Supplementary Fig. 4) before next round of immunolabeling. By repeating the steps, we performed continuous six rounds of immunolabeling on the same MOCAT-processed adult mouse brain. For each round, the brain was labeled with lectin as a structural reference, and one antibody specific for a target protein (Fig. 2b). The six antibody image data sets were then registered and aligned using Elastix[23] to generate a multichannel image (Fig 2c). These results demonstrated spatial distribution of different neuronal markers and the compatibility of MOCAT with various primary antibodies.

MOCAT preserves the proteomic expressional changes caused by disease and therapy

Volumetric imaging is vital for disease researches because it offers precise microenvironment spatial information and therapy effect evaluation[17,24,25]. To examine the applicability of MOCAT to disease researches, we first applied MOCAT to an adult mouse brain of the astrocytoma mouse model (see Methods) to label the tumor cells and astrocytes (Fig. 3a and c). Astrocytes surrounding the tumor were segmented (Fig. 3b, d and e) and classified by their cell-to-tumor distances. The statistics (Fig. 3f) showed that almost half of astrocytes located within the tumor, and 63.9% of the astrocytes located close to the tumor surface (within the range of ± 200 µm). Our results showed that the image data sets of MOCAT can be used to analyze cell distribution and reveal the spatial architecture of a disease microenvironment. We then used a mouse model of traumatic brain injury (TBI) to compare the quantification results of MOCAT-processed and SDS-delipidated mouse brains. Studies have reported that TBI disrupts dopamine neurotransmission, reduces dopamine levels, and causes cell loss in the nigrostriatal

bioRxiv preprint doi: https://doi.org/10.1101/2022.11.28.518189; this version posted December 2, 2022. The copyright holder for this preprint (which was not certified by peer review) is the author/funder. All rights reserved. No reuse allowed without permission.

system[26,27]. Therefore, we use TH antibodies to label the dopaminergic system (Fig. 4a). We found that the injury side of the brain showed striatal morphological extension and distortion in both SDS-delipidated (Supplementary Fig. 5) and MOCAT (Fig. 4b) processed samples, implying a possible malfunction or imbalance in the dopaminergic system. To assess the damage, we segmented the striatum (Fig. 4b), nigrostriatal fiber tracts (Fig. 4c) and the dopaminergic neuronal cells in the substantia nigra (Fig. 4d) and calculate the relative volumes and cell numbers of injury side to contralateral side. We found that the injury side of both MOCAT and SDS-delipidated TBI brain showed approximately 20%, 30%, and 15% reduction in striatal volume, nigrostriatal fiber tract volume, and cell number of substantia nigra, respectively, compared to the contralateral side (Fig. 4e), indicating that neuronal damage was preserved and could be assessed using FFPE samples. Next, we evaluated the therapeutic effect of a nitrogen oxide producing nanoparticle (aNORO, See Methods) on angiogenesis. We segmented an area of blood vessels directly beneath the injury site of both sham and aNORO-received mouse brains (Fig. 4f and Supplementary Fig. 6) and calculated the volume, surface area, length, and number of bifurcations to assess angiogenesis (see Methods). The results of both MOCAT and SDS-delipidated brains indicated that the mouse receiving aNORO injection exhibited approximately 60% improvement in angiogenesis compared to the sham group (Fig. 4g). Taken together, MOCAT preserves structural and proteomic expressional changes and can be used to evaluate the effect of therapy and behavioral experiments.

Application of MOCAT to human brain tissue facilitates study of complexed microenvironment

While the concept of long-term archiving mouse brains for future intact imaging is still new, human brain sample preservation has been performed in human brain tissue banks worldwide. In most research centers, collected tissues are stored unfixed at −70°C to −85°C or in 10% formalin at room temperature. However, ultralow temperature preservation requires a lot of space and energy, and long-term storage in formalin impedes aqueous-based delipidation[18,28] and reduces the tissue's antigenicity[29], preventing scientists from performing whole-mount immunolabeling and 3D visualization. To demonstrate the applicability of MOCAT to human brain tissues, we applied this method to a human brain tissue sample collected surgically from the temporal lobe and compared immunolabeling results with the results of formalin-preserved brain blocks stored for 1 year and 45 days (see Methods). The astrocytic foot processes were stained in the brain specimen stored in an FFPE block for 60 days but not in the formalin-preserved brain blocks stored for 1 year and 45 days (Fig. 4a), indicating that FFPE is superior to formalin for antigenicity preservation. On the same sample, we then performed two additional rounds of immunolabeling to axons

bioRxiv preprint doi: https://doi.org/10.1101/2022.11.28.518189; this version posted December 2, 2022. The copyright holder for this preprint (which was not certified by peer review) is the author/funder. All rights reserved. No reuse allowed without permission.

and dendrites, respectively (Fig. 4b). The image data sets from each round could be registered into a single multichannel image with lectin-labeled blood vessels as a reference channel (Fig. 4c), enabling us to reconstruct the relationship between these biomarkers.

Discussion

In this study, we present a paraffin-embedding processing-based technique that combines sample preservation and sample delipidation. Some studies have performed tissue-clearing methods on FFPE specimens[28,30–34], but they only considered FFPE tissues as a specimen type. No attempt has been made to exploit the characteristics of FFPE processing in large tissue clearing. In studies applying tissue clearing and immunolabeling on FFPE samples, researchers have subjected dewaxed FFPE samples to additional delipidation steps, such as CUBIC[31], iDISCO[30,32,33], and SDS-based delipidation[24,28] to remove remained lipids. In our experiments, we found that the heat-induced antigen retrieval is sufficient to remove residual lipids in dewaxed FFPE samples. Notably, delipidation at room temperature cannot replace heat-induced antigen retrieval for whole-mount immunolabeling FFPE samples. In our preliminary immunolabeling experiment with tyrosine hydroxylase antibody, the SDS-delipidated FFPE mouse brain (without heat-treatment) exhibited weaker signals and noticeable nonspecific background noises (Supplementary Fig. 7). Such phenomenon was observed in FFPE tissue sections with inadequate antigen retrieval[30]. In conclusion, heat-induced antigen retrieval is a crucial step that has the effect of but cannot be replaced by delipidation for FFPE tissue immunolabeling.

For the samples that have no need to be archived, MOCAT can work as a fast delipidation method via simple dehydration, xylene clearing and antigen retrieval. Compared with other organic solvent-based large tissue clearing methods, such as 3DISCO and iDISCO, MOCAT processing is easy to perform in hospitals and research institutes, and the necessary solvents (ethanol and xylene) are less expensive and more readily available. Endogenous fluorescent proteins are easily quenched in ethanol, but they can still be visualized through immunolabeling.

MOCAT is applicable to aged FFPE blocks and enables repeated immunolabeling on the same specimen, compensating for the rarity of clinical human brain specimens. Therefore, MOCAT is a powerful tool for clinical brain research, including the investigation of the microenvironment surrounding lesions. To achieve this purpose, we require computational tools for the registration and alignment of multiplex data sets.

bioRxiv preprint doi: https://doi.org/10.1101/2022.11.28.518189; this version posted December 2, 2022. The copyright holder for this preprint (which was not certified by peer review) is the author/funder. All rights reserved. No reuse allowed without permission.

The published tools, such as Advanced Normalization Tools (ANTs)[35] and Elastix[23], are suitable for use in specimens with clear boundaries, such as intact mouse brains. However, the registration is unsatisfactory for a patient-obtained piece of human brain tissue, which typically has broken boundaries and irregular shapes. Therefore, developing an algorithm for the registration of large-size data sets from irregular shaped sample is essential for volumetric human brain imaging in the future.

The strong autofluorescence caused by blood cells and lipofuscin is another challenge for 3D visualization of a human brain sample. Protocols reported being effective on tissue sections to eliminate the auto-fluorescence, such as $CuSO_4$[36] and photobleaching[37], only weaken the autofluorescence in large human tissue in our hands. Some studies have used H_2O_2[38], which is unsuitable for large tissue because prolonged immersion time may affect antigenicity. An alternative method utilizing spectral imaging and linear unmixing was reported for identifying and removing autofluorescence in brain tissue sections[39]; this method has the potential to be modified and applied to large tissues.

In conclusion, this study presents MOCAT, a method for quickly preserving and delipidating biological samples for whole-mount immunolabeling and 3D visualization. Furthermore, this method enables long-term sample preservation at room temperature without antigenicity loss and multiple rounds of immunolabeling. Therefore, MOCAT maximizes the use of archived tissues and facilitates future studies in 3D mappings, such as connectomics.

Methods

Experimental animals and human samples

We used 8-week-old CD-1 male mice for MOCAT pipeline development. All animal procedures and handlings complied with the guideline from the Institutional Animal Care and Use Committee of Academia Sinica (IACUC protocol No.: 12-05-370), Taiwan. Experimental mice information for astrocytoma and TBI mouse models is described below. The postmortem human brain samples were provided by Dr. Hwai-Jong Cheng. The studies involving human participants were reviewed and approved by the Institutional Review Board of National Taiwan University Hospital (IRB No.: 202203079RINC), and the participants provided signed informed consent.

Astrocytoma animal model

All animal procedures and handlings complied with the guideline from the Institutional

bioRxiv preprint doi: https://doi.org/10.1101/2022.11.28.518189; this version posted December 2, 2022. The copyright holder for this preprint (which was not certified by peer review) is the author/funder. All rights reserved. No reuse allowed without permission.

Animal Care and Use Committee of National Tsing Hua University (IACUC protocol No.: 109067), Taiwan. ALTS1C1-GFP cells (1×10^5 cells) were implanted into the brains of 8-week-old C57BL/6 mice following the procedure published[40]. Briefly, under anesthesia, 1×10^5 ALTS1C1-GFP cells were injected with a 2.5-mm depth at 2 mm laterals to the midline and 1 mm posterior to the bregma. After injection, bone wax (ETHICON, W810, Somerville, NJ, USA) was applied to seal the drilled hole. Eighteen days after the tumor implantation, mice were sacrificed after cardiac perfusion.

TBI mouse model

All animal procedures and handlings complied with the guideline from the Institutional Animal Care and Use Committee of National Tsing Hua University (IACUC protocol No.: 110081). We divided 7-week-old C57BL/6 female mice into two groups: (1) untreated (sham) and (2) treated with alternating magnetic field-responsive NO-release octahedrons (aNORO@sMN). When applying TBI to mice, we used an electric drill to create a hole in the skull. The TBI site was on the left motor cortex (M1 & M2). A 2-mm-diameter punch was then used to cause a 1.5-mm-deep injury. For the treated group, the NO-release octahedrons (aNORO) were embedded in a silk microneedle (sMN). The microneedle was implanted one day postinjury to avoid excessive swelling in the injured area. The mice were sacrificed 45 days after the TBI induction.

MOCAT

The MOCAT workflow is presented in Fig. 1a. The details are provided below.

Sample preparation. The mice were perfused with 20 mL of cold phosphate-buffered saline (PBS) and then 20 mL of 4% PFA. The collected brains were further fixed using 4% PFA at 4°C for 24 hours. The PFA-fixed brains were dehydrated, processed in a tissue processer (The Tissue-Tek VIP 5 Jr., Sakura Finetek Japan Co., Ltd., Japan), and embedded in paraffin wax. The FFPE brains were stored at room temperature.

Deparaffination and rehydration. The FFPE brains were incubated at 65°C to melt paraffin. Residual paraffin was removed through immersion in xylene for 24 hours. Xylene was changed at least twice. Dewaxed brains were rehydrated with 100%, 100%, 95%, 85%, 75%, and 55% alcohol diluted with distilled water. The rehydrated brains were then washed with PBS.

SHIELD procedure. The dewaxed and rehydrated brains were treated with epoxy following the published SHIELD protocol[22]. The brains were incubated in the SHIELD-OFF solution at 4°C for four days, followed by one more day in the SHIELD-ON solution at

bioRxiv preprint doi: https://doi.org/10.1101/2022.11.28.518189; this version posted December 2, 2022. The copyright holder for this preprint (which was not certified by peer review) is the author/funder. All rights reserved. No reuse allowed without permission.

37°C. All reagents were prepared from SHIELD kits (LifeCanvas Technologies, Seoul, South Korea) according to the manufacturer's instructions.

Antigen retrieval. The SHIELD-processed brains were incubated overnight at 4°C in a modified citrate buffer (10 mM sodium citrate, 1% Triton X-100, pH 6.0). The brains and buffer were warmed to room temperature and cooked for 6 min at 121°C in a pressure cooker (Bio SB, Santa Barbara, CA, USA). The brains and buffer were kept in the pressure cooker until the temperature dropped below 100°C (for approximately 15 min). Next, the brains were removed from the cooker and allowed to cool for 10 min at room temperature. The brains were then washed in PBST (1× PBS with 0.1% Triton X-100) 3 times, with 1 hour per wash.

Electrophoretic immunolabeling. The procedure was modified from the published eFLASH protocol[11] and conducted in the SmartLabel System (LifeCanvas Technologies, Seoul, South Korea). The brains were preincubated overnight at room temperature in sample buffer (240 mM Tris, 160 mM CAPS, 20% w/v D-sorbitol, 0.9% w/v sodium deoxycholate). Each preincubated brain was placed in a sample cup (provided by the manufacturer with the SmartLabel System) containing primary and corresponding secondary antibodies diluted in 8 mL of sample buffer. Antibody information and optimized quantity are detailed in Supplementary Table 1. The sample cup and 500 mL of labeling buffer (240 mM Tris, 160 mM CAPS, 20% w/v D-sorbitol, 0.2% w/v sodium deoxycholate) were loaded into the SmartLabel System. The device was operated at a constant voltage of 90 V with a current limit of 400 mA. After 18 hours of electrophoresis, we added 300 mL of booster solution (20% w/v D-sorbitol, 60 mM boric acid), and electrophoresis was continued for 4 hours. Immunolabeled brains were washed with PTwH[9] (1× PBS with 0.2% w/v Tween-20 and 10 µg/mL heparin) 2 times, with 3 hours per wash, and then postfixed with 4% PFA at room temperature for 1 day. The brains were washed with PBST 2 times, with 3 hours per wash, to remove any residual PFA.

Refractive index (RI)-matching. Before imaging, the brains were RI-matched by immersing them in NFC1 and NFC2 solutions (Nebulum, Taipei, Taiwan) for 1 day at room temperature.

Volumetric imaging and 3D visualization. The whole mouse brain was imaged using a light-sheet microscope (SmartSPIM, LifeCanvas Technologies, Seoul, South Korea). For less-than-3-mm-thick samples, imaging was performed using a multipoint confocal microscope (Andor Dragonfly 200, Oxford Instruments, UK). 3D visualization was

bioRxiv preprint doi: https://doi.org/10.1101/2022.11.28.518189; this version posted December 2, 2022. The copyright holder for this preprint (which was not certified by peer review) is the author/funder. All rights reserved. No reuse allowed without permission.

performed using Imaris software (Imaris 9.5.0, Bitplane, Belfast, UK).

Photobleaching. The immunolabeled and imaged brain was placed in a multiwell plate and immersed in RI-matching solutions to keep it transparent. The plate was sealed with paraffin. A 100-W projection lamp with an LED array was placed on the plate to quench the fluorescent signals. A representative photobleaching apparatus constructed using off-the-shelf components is shown in Supplementary Fig. 8. For a 2-mm-thick sample, 18 hours of photobleaching was sufficient.

SDS-delipidation

The mice were perfused with 20 mL of cold phosphate-buffered saline (PBS) and then 20 mL of 4% PFA. The brains were collected and further fixed in 4% PFA at 4°C for 24 hours. The fixed brains were treated with SHIELD procedure described in previous session. The SHIELD-processed brains were cleared using stochastic electro-transport (SmartClear Pro II, LifeCanvas Technologies, Seoul, South Korea) with a constant current 1.2 A for 5-7 days. The cleared brains were washed with PBST (1X phosphate-buffered saline containing 0.1% triton X-100 detergent) at room temperature for at least overnight.

Raman microscopy

A Yb:KGW laser (Carbide, Light Conversion) emitting 190 fs, 200 kHz, 20 W pulse train at 1030 nm wavelength is used to generate supercontinuum via a double-pass multiple-plate continuum module[41]. The resulting spectrum (600-1300 nm) is spectrally sliced by tunable color filters (3G LVLWP, LVSWP, and LVFBP, Delta) to provide pump (725 nm) and Stokes (914 nm) beams, which can address the Raman shift (2850 cm^{-1}) of lipids. The two beams are temporally and spatially overlapped, then guided into a commercial upright microscope (Axio Examiner.Z1, Zeiss) with a scanning unit (LSM7MP, Zeiss) to achieve raster scanning on the x-y plane. A single 20x water immersion objective (UMPLFLN 20XW, Olympus) is used to focus the combined laser beams on the mouse sample. Epi-CARS signal at 601 nm is spectrally separated from the incident radiation with a bandpass filter (BP 565-610, Zeiss) and detected by a photomultiplier tube. The mean gray value is calculated via ImageJ.

Multichannel image registration

For the 6-round immunolabeling of a single whole mouse brain, the data sets of each round contain one structural channel stained with lectin and one antibody-stained channel. The image data set of the first staining round was used as a standard brain. The lectin channel images of each other data set were registered to the lectin channel of the standard brain through Elastix toolbox[23]. Transformation parameters obtained from rigid

bioRxiv preprint doi: https://doi.org/10.1101/2022.11.28.518189; this version posted December 2, 2022. The copyright holder for this preprint (which was not certified by peer review) is the author/funder. All rights reserved. No reuse allowed without permission.

and B-spline deformable registration were applied to the antibody-stained channels. Transformed images were merged and visualized using Imaris software. For the human specimen, the image data sets of three rounds were registered and resampled using Amira software (Thermo Fisher Scientific, Waltham, MA, USA). Resampled images were merged and visualized using Imaris software.

Quantification and statistics

For volume and surface area quantification, we used the Surface function of Imaris software to segment the striatum, nigrostriatal fiber tracts, and blood vessels in the selected regions of interest. For cell number quantification, the area of substantia nigra (SN) was masked out using Surface, and the cells within SN were detected using the Spot function of Imaris. For calculating the bifurcations and length of blood vessels, we used the feature extraction method provided by Vessap[42] to detect the centerlines of the blood vessels and the bifurcation point. First, erosion and dilation were performed to remove false-negative pixels and avoid false centerline detections. Next, the centerlines were extracted with a 3D thinning algorithm[43], and the bifurcation points were detected using the surrounding pixels of each point to decide a point that splits into two or more vessels. All statistical analyses were performed using GraphPad Prism (GraphPad Software Inc., San Diego, CA, USA).

Antigen retrieval test

The brains were collected and processed as described in the MOCAT section of Methods. Four conditions were tested: (1) Heat-induced retrieval in pH 6.0 solution; (2) Heat-induced retrieval in pH 9.0 solution; (3) SDS at room temperature; (4) No antigen retrieval. For condition 1, the dewaxed, SHIELD-processed brain was incubated overnight at 4°C in citrate buffer (10 mM sodium citrate, 1% Triton X-100, pH 6.0). The brains and buffer were then warmed to room temperature and cooked for 6 min at 121°C in a pressure cooker (Bio SB, Santa Barbara, CA, USA). For condition 2, a commercial Tris-EDTA buffer (ab93684, Abcam, Cambridge, UK) was used following the procedure in condition 1. For condition 3, SDS-based electrophoresis was performed using stochastic electrotransport (SmartClear Pro II, LifeCanvas Technologies, Seoul, South Korea) with a constant current of 1.2 A for 2 days. Finally, for condition 4, the dewaxed, SHIELD-processed brain directly proceeded to the immunolabeling step.

bioRxiv preprint doi: https://doi.org/10.1101/2022.11.28.518189; this version posted December 2, 2022. The copyright holder for this preprint (which was not certified by peer review) is the author/funder. All rights reserved. No reuse allowed without permission.

References

1. Chung, K. *et al.* Structural and molecular interrogation of intact biological systems. *Nature* **497**, 332–337 (2013).
2. Ertürk, A. *et al.* Three-dimensional imaging of solvent-cleared organs using 3DISCO. *Nat. Protoc.* **7**, 1983–1995 (2012).
3. Tainaka, K. *et al.* Chemical Landscape for Tissue Clearing Based on Hydrophilic Reagents. *Cell Rep.* **24**, 2196-2210.e9 (2018).
4. Ueda, H. R. *et al.* Tissue clearing and its applications in neuroscience. *Nature Reviews Neuroscience* vol. 21 61–79 (2020).
5. Tian, T., Yang, Z. &Li, X. Tissue clearing technique: Recent progress and biomedical applications. *J. Anat.* **238**, 489–507 (2021).
6. Yu, T., Zhu, J., Li, D. &Zhu, D. Physical and chemical mechanisms of tissue optical clearing. *iScience* **24**, 102178 (2021).
7. Kim, S. Y. *et al.* Stochastic electrotransport selectively enhances the transport of highly electromobile molecules. *Proc. Natl. Acad. Sci. U. S. A.* **112**, E6274–E6283 (2015).
8. Hama, H. *et al.* Scale: A chemical approach for fluorescence imaging and reconstruction of transparent mouse brain. *Nat. Neurosci.* **14**, 1481–1488 (2011).
9. Renier, N. *et al.* IDISCO: A simple, rapid method to immunolabel large tissue samples for volume imaging. *Cell* **159**, 896–910 (2014).
10. Murakami, T. C. *et al.* A three-dimensional single-cell-resolution whole-brain atlas using CUBIC-X expansion microscopy and tissue clearing. *Nat. Neurosci.* **21**, 625–637 (2018).
11. Yun, D. H. *et al.* Ultrafast immunostaining of organ-scale tissues for scalable proteomic phenotyping. *bioRxiv* 660373 (2019) doi:10.1101/660373.
12. Susaki, E. A. *et al.* Versatile whole-organ/body staining and imaging based on electrolyte-gel properties of biological tissues. *Nat. Commun. 2020 111* **11**, 1–22 (2020).
13. Navabpour, S., Kwapis, J. L. &Jarome, T. J. A neuroscientist's guide to transgenic mice and other genetic tools. *Neurosci. Biobehav. Rev.* **108**, 732–748 (2020).
14. Roy, D. S. *et al.* Brain-wide mapping reveals that engrams for a single memory are distributed across multiple brain regions. *Nat. Commun. 2022 131* **13**, 1–16 (2022).
15. Roostalu, U. *et al.* Quantitative whole-brain 3D imaging of tyrosine hydroxylase-labeled neuron architecture in the mouse MPTP model of Parkinson's disease. *DMM Dis. Model. Mech.* **12**, (2019).
16. Renier, N. *et al.* Mapping of Brain Activity by Automated Volume Analysis of Immediate Early Genes. *Cell* **165**, 1789–1802 (2016).
17. Liebmann, T. *et al.* Three-Dimensional Study of Alzheimer's Disease Hallmarks Using the iDISCO Clearing Method. *Cell Rep.* **16**, 1138–1152 (2016).
18. Muntifering, M. *et al.* Clearing for Deep Tissue Imaging. *Curr. Protoc. Cytom.* **86**, e38 (2018).

bioRxiv preprint doi: https://doi.org/10.1101/2022.11.28.518189; this version posted December 2, 2022. The copyright holder for this preprint (which was not certified by peer review) is the author/funder. All rights reserved. No reuse allowed without permission.

19. Shi, S. R. *et al.* Evaluation of the value of frozen tissue section used as 'gold standard' for immunohistochemistry. *Am. J. Clin. Pathol.* **129**, 358–366 (2008).
20. Denti, V. *et al.* Antigen Retrieval and Its Effect on the MALDI-MSI of Lipids in Formalin-Fixed Paraffin-Embedded Tissue. *J. Am. Soc. Mass Spectrom.* **31**, 1619–1624 (2020).
21. Shi, S. R., Shi, Y. &Taylor, C. R. Antigen retrieval immunohistochemistry: Review and future prospects in research and diagnosis over two decades. *Journal of Histochemistry and Cytochemistry* vol. 59 13–32 (2011).
22. Park, Y.-G. *et al.* Protection of tissue physicochemical properties using polyfunctional crosslinkers. *Nat. Biotechnol.* **37**, 73–83 (2019).
23. Klein, S., Staring, M., Murphy, K., Viergever, M. A. &Pluim, J. P. W. elastix: a toolbox for intensity-based medical image registration. *IEEE Trans. Med. Imaging* **29**, 196–205 (2010).
24. Chen, Y. *et al.* Three-dimensional imaging and quantitative analysis in CLARITY processed breast cancer tissues. *Sci. Rep.* **9**, 1–13 (2019).
25. Gómez-Gaviro, M. V., Sanderson, D., Ripoll, J. &Desco, M. Biomedical Applications of Tissue Clearing and Three-Dimensional Imaging in Health and Disease. *iScience* **23**, 101432 (2020).
26. PO, J. *et al.* Dopaminergic abnormalities following traumatic brain injury. *Brain* **141**, 797–810 (2018).
27. Verduzco-Mendoza, A. *et al.* Role of the Dopaminergic System in the Striatum and Its Association With Functional Recovery or Rehabilitation After Brain Injury. *Front. Neurosci.* **0**, 783 (2021).
28. Lai, H. M. *et al.* Next generation histology methods for three-dimensional imaging of fresh and archival human brain tissues. doi:10.1038/s41467-018-03359-w.
29. Thavarajah, R., Mudimbaimannar, V. K., Elizabeth, J., Rao, U. K. &Ranganathan, K. Chemical and physical basics of routine formaldehyde fixation. *J. Oral Maxillofac. Pathol.* **16**, 400 (2012).
30. vanRoyen, M. E. *et al.* Three-dimensional microscopic analysis of clinical prostate specimens. *Histopathology* **69**, 985–992 (2016).
31. Nojima, S. *et al.* CUBIC pathology: Three-dimensional imaging for pathological diagnosis. *Sci. Rep.* **7**, 1–14 (2017).
32. Tanaka, N. *et al.* Whole-tissue biopsy phenotyping of three-dimensional tumours reveals patterns of cancer heterogeneity. *Nat. Biomed. Eng.* **1**, 796–806 (2017).
33. Tanaka, N. *et al.* Mapping of the three-dimensional lymphatic microvasculature in bladder tumours using light-sheet microscopy. *Br. J. Cancer 2018 1187* **118**, 995–999 (2018).
34. Lloyd-Lewis, B. *et al.* Imaging the mammary gland and mammary tumours in 3D: Optical tissue clearing and immunofluorescence methods. *Breast Cancer Res.* **18**, 1–17 (2016).
35. Susaki, E. A. *et al.* Whole-brain imaging with single-cell resolution using chemical

bioRxiv preprint doi: https://doi.org/10.1101/2022.11.28.518189; this version posted December 2, 2022. The copyright holder for this preprint (which was not certified by peer review) is the author/funder. All rights reserved. No reuse allowed without permission.

cocktails and computational analysis. *Cell* **157**, 726–739 (2014).

36. Md. Mahmudul Alam*, K. J. and D. P. Potential application of CuSO4 for the reduction of lipofuscin autofluorescence in formalin-fixed paraffin-embedded tissue. *Bioresearch Commun.* **2**, 170–174 (2016).
37. Sun, Y., Ip, P. &Chakrabartty, A. Simple Elimination of Background Fluorescence in Formalin-Fixed Human Brain Tissue for Immunofluorescence Microscopy. *J. Vis. Exp.* **2017**, 56188 (2017).
38. Zeller, P., Ploux, O. &Méjean, A. A simple protocol for attenuating the auto-fluorescence of cyanobacteria for optimized fluorescence in situ hybridization (FISH) imaging. *J. Microbiol. Methods* **122**, 16–19 (2016).
39. Pyon, W. S., Gray, D. T. &Barnes, C. A. An alternative to dye-based approaches to remove background autofluorescence from primate brain tissue. *Front. Neuroanat.* **13**, 73 (2019).
40. Wang, S. C., Hong, J. H., Hsueh, C. &Chiang, C. S. Tumor-secreted SDF-1 promotes glioma invasiveness and TAM tropism toward hypoxia in a murine astrocytoma model. *Lab. Invest.* **92**, 151–162 (2012).
41. Huang, G.-J. *et al.* Towards stimulated Raman scattering spectro-microscopy across the entire Raman active region using a multiple-plate continuum. *Opt. Express, Vol. 30, Issue 21, pp. 38975-38984* **30**, 38975–38984 (2022).
42. Todorov, M. I. *et al.* Machine learning analysis of whole mouse brain vasculature. *Nat. Methods 2020 174* **17**, 442–449 (2020).
43. Lee, T. C., Kashyap, R. L. &Chu, C. N. Building Skeleton Models via 3-D Medial Surface Axis Thinning Algorithms. *CVGIP Graph. Model. Image Process.* **56**, 462–478 (1994).

Acknowledgments

We thank the Brain Research Center, National Tsing-Hua University, Taiwan and Pathology core, Institute of Biomedical Sciences, Academia Sinica, Taiwan for the technical assistance. This work was funded by the grants from National Science and Technology Council (NSTC-111-2636-B-007-007, NSTC-07-2314-B-007-003-MY3, NSTC-111-2321-B-002-016). This work was also supported by the Brain Research Center under the Higher Education Sprout Project, co-funded by the Ministry of Education and the National Science and Technology Council in Taiwan.

Author information

Contributions

Y.H.L., B.C.C. and L.A.C. conceived the study and designed the experiments. Y.H.C. prepared FFPE samples. Y.H.L. performed immunostaining, imaging and image visualization. Y.H.L. and L.W.W. performed image data analysis. Y.C.C. and S.H.H. provided TBI-induced mice. S.Y.W. and

bioRxiv preprint doi: https://doi.org/10.1101/2022.11.28.518189; this version posted December 2, 2022. The copyright holder for this preprint (which was not certified by peer review) is the author/funder. All rights reserved. No reuse allowed without permission.

C.S.C. provided the tumor-implanted mice. S.D.Y. performed Raman microscopy. S.T.H., K.C.W., C.H.L. and H.J.C. provided the human brain tissues. Y.H.L. and L.A.C. wrote the manuscript.

Corresponding authors

Correspondence to Li-An Chu and Bi-Chang Chen

Ethics declarations

Competing interests

The authors declare no competing interests.

bioRxiv preprint doi: https://doi.org/10.1101/2022.11.28.518189; this version posted December 2, 2022. The copyright holder for this preprint (which was not certified by peer review) is the author/funder. All rights reserved. No reuse allowed without permission.

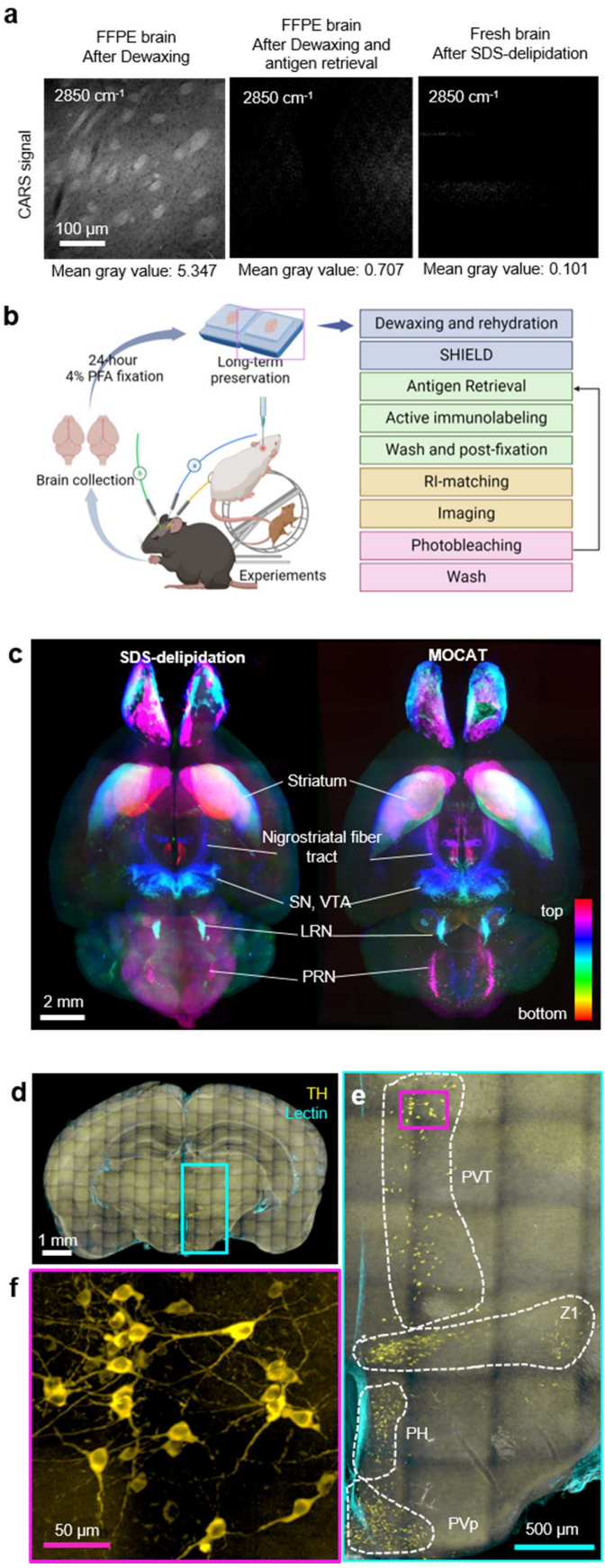

Fig. 1: MOCAT reveals the three-dimensional (3D) biomarker expression pattern of a whole FFPE mouse brain. a, Images of coherent anti-Stokes Raman scattering (CARS) of dewaxed FFPE mouse brain without antigen retrieval; dewaxed FFPE mouse brain with antigen retrieval and freshly prepared SDS-delipidated mouse brain. The images were taken at Raman shift of 2850 cm^{-1} to address the CH2 vibration frequency. The mean gray values were shown below images. **b,** The MOCAT workflow. **c,** Brain-wide tyrosine hydroxylase (TH) expression in FFPE and fresh wild-type C57BL/6 mice. The expression patterns are shown in temporal code. The major dopaminergic regions are identified. SN, substantia nigra; VTA, ventral tegmental area; LRN, lateral reticular nucleus; PRN, pontine reticular nucleus. **d,** Application of MOCAT to a 15-year-old FFPE block. Top-left: The projection image of a 2-mm-thick mouse brain slice retrieved from the 15-year-old FFPE block. **e,** Magnification of the region marked in **d.** The dopaminergic regions are identified. PVT, paraventricular nucleus of thalamus; PH, posterior hypothalamic nucleus; PVp, periventricular hypothalamic nucleus. **f,** Magnification of the region marked in **e**. Scale bars are indicated on each figure.

bioRxiv preprint doi: https://doi.org/10.1101/2022.11.28.518189; this version posted December 2, 2022. The copyright holder for this preprint (which was not certified by peer review) is the author/funder. All rights reserved. No reuse allowed without permission.

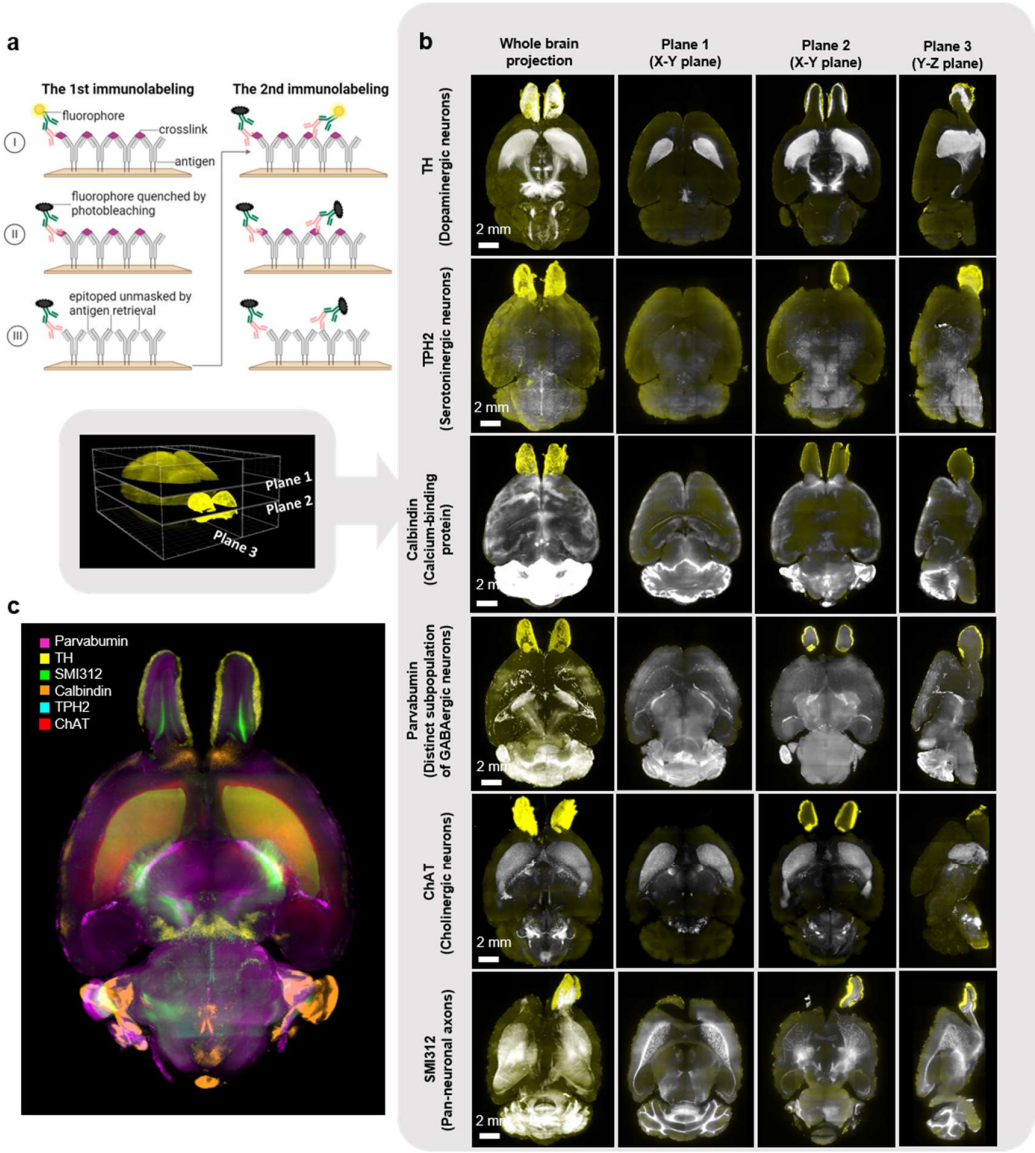

Fig. 2: MOCAT enables multiple rounds of whole-brain immunostaining. a, A schematic of the photobleaching and antigen retrieval steps. **b,** The image data sets of 6-round immunolabeling. Two X–Y planes (different z-positions) and one Y–Z plane are shown. **c,** The merged multichannel image.

bioRxiv preprint doi: https://doi.org/10.1101/2022.11.28.518189; this version posted December 2, 2022. The copyright holder for this preprint (which was not certified by peer review) is the author/funder. All rights reserved. No reuse allowed without permission.

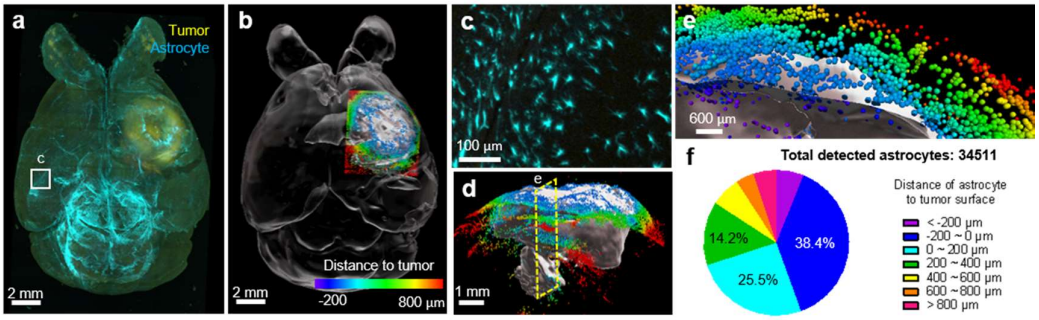

Fig. 3: MOCAT reveals cell-tumor relationship in an astrocytoma model. a, The projection image of a MOCAT-processed mouse brain with xenograft astrocytoma (ALTS1C1 cells, see Methods). **b,** Segmented mouse brain with tumor (white) and surrounding astrocytes. The astrocytes are colored in cell-to-tumor distance-code. **c,** The magnification of the region marked in **a**, showing the morphology of astrocytes. **d,** The sagittal view of the segmented tumor and color-coded astrocytes. **e,** The magnification of the clipping plane marked in **d**, showing astrocytes inside (dark blue, purple) and outside the tumor. **f,** Quantification of the detected astrocytes and classification according to their distance to tumor surface.

bioRxiv preprint doi: https://doi.org/10.1101/2022.11.28.518189; this version posted December 2, 2022. The copyright holder for this preprint (which was not certified by peer review) is the author/funder. All rights reserved. No reuse allowed without permission.

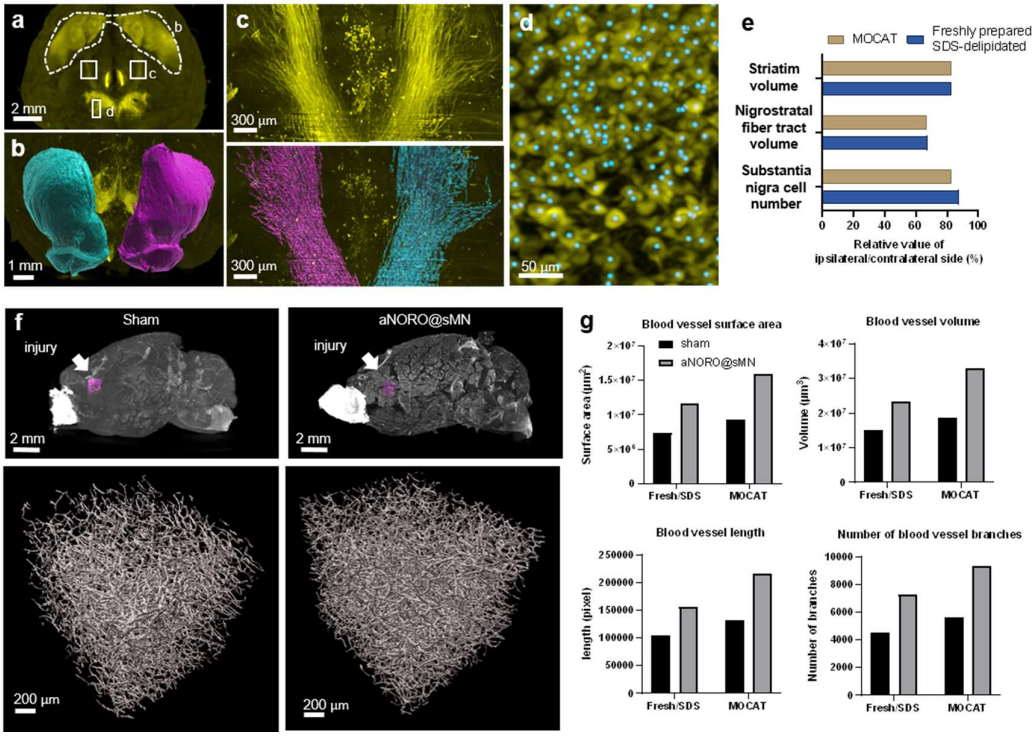

Fig. 4: MOCAT demonstrates damage and therapeutic effect of NO-released particles in TBI mouse model. a, Fluorescent image of TH immunolabeling. **b,** Frontal view of segmented striatum (dot line circled in **a**). Magenta: the injury side; cyan: the contralateral side. **c,** The horizontal views of the nigrostriatal fiber tract (marked in **a**); fluorescent and segmented images are shown (upper and bottom in order). Magenta: the injury side; cyan: the contralateral side. **d,** Detection of dopaminergic cells in substantia nigra (SN). Magnification of the marked area in **a**, including the original TH fluorescent signal (yellow) and segmented cell spots (cyan dots), is shown. **e,** Quantification of striatum volume, nigrostriatal volume, and substantia nigra cell number. The relative ipsilateral/contralateral values are shown. **f,** Reconstruction of blood vessels in TBI brains with and without treatments. The regions of interested (ROIs) selected for assessment of angiogenesis were indicated in the upper row (magenta boxes, right below the injury site). The 3D reconstructions of blood vessels were shown in the bottom row. **g,** Quantification of blood vessel volume, blood vessel surface area, number of blood vessel branches, and blood vessel length. Both of the MOCAT- and SHIELD-processed aNORO@sMN-treated group (see Methods) shows approximately 60% improvements compared with the sham group.

bioRxiv preprint doi: https://doi.org/10.1101/2022.11.28.518189; this version posted December 2, 2022. The copyright holder for this preprint (which was not certified by peer review) is the author/funder. All rights reserved. No reuse allowed without permission.

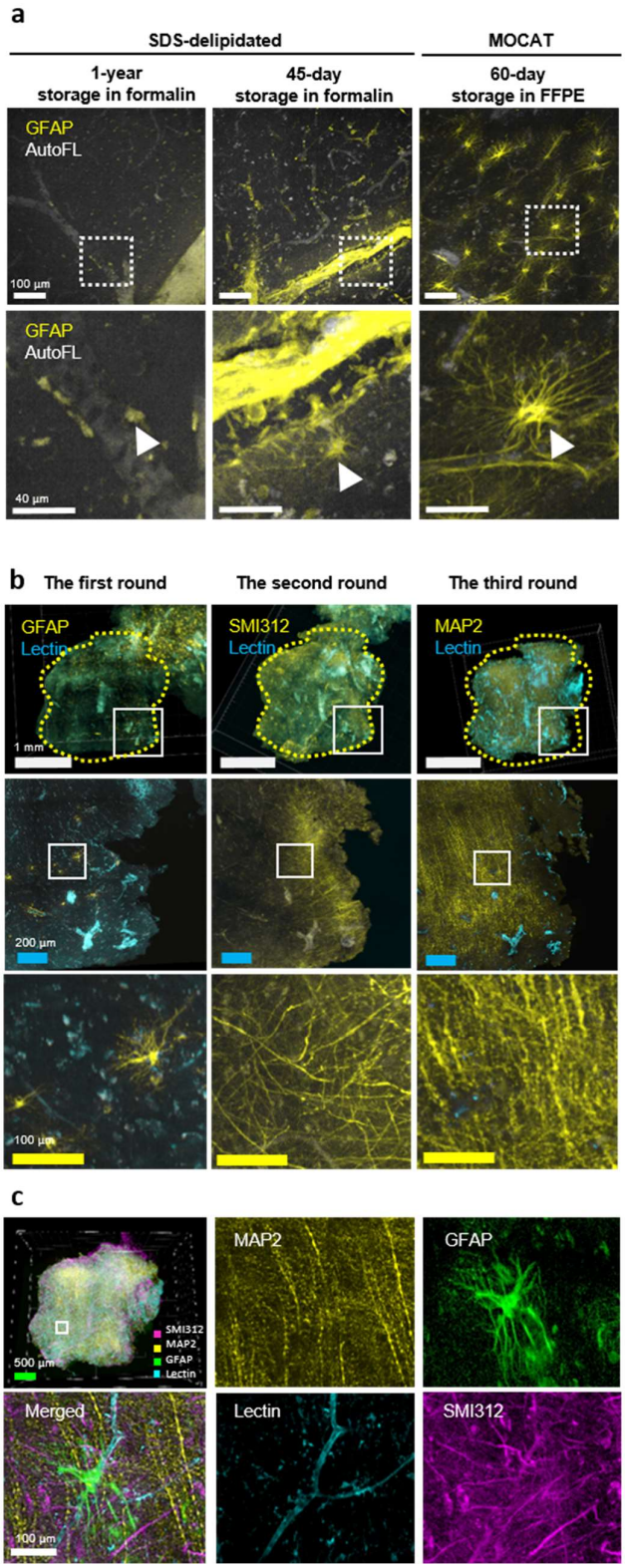

Fig. 5: Application of MOCAT to human brain tissue. a, Immunolabeling of glial fibrillary acidic protein (GFAP; the astrocyte marker). Human brain tissues stored in formalin or FFPE blocks are cleared and immunolabeled. Stained astrocytes are indicated by arrowheads in the bottom row. **b,** Three rounds of immunolabeling were performed sequentially on the same human brain tissue. For each round, one neuronal marker and lectin were used. The upper row presents the projection images of the whole tissue. The middle row presents one optical section of the boxed area in the upper row. The bottom row shows the magnification of the boxed area indicated in the middle row. GFAP: Glial fibrillary acidic protein; SMI312: pan-axonal marker; MAP2: microtubule-associated protein 2, a dendritic marker. **c,** The merged multichannel images. The projection image of the whole tissue, and the images of merged and single channels of one optical section of the selected area (white box) are shown.